Stress hot spots in viscoplastic deformation of polycrystals

Stress hot spots in viscoplastic deformation of polycrystals

A D Rollett[1], R A Lebensohn[2], M Groeber[3], Y Choi[4], J Li[1] and G S Rohrer[1]

[1] Materials Science and Engineering Department, Carnegie Mellon University Pittsburgh PA 15213; 412-268-3177, USA
[2] Materials Science and Technology Division, Los Alamos National Laboratory, Los Alamos, NM 87845, USA
[3] AFRL/RXLM Bldg 655, 2230 Tenth Street, Wright-Patterson AFB, OH 45433-7817, USA
[4] UES, Inc., 4401 Dayton-Xenia Rd., Dayton, OH 45432-1894, USA

E-mail: Rollett@andrew.cmu.edu

Abstract

The viscoplastic deformation of polycrystals under uniaxial loading is investigated to determine the relationship between hot spots in stress and their location in relation to the microstructure. A 3D full-field formulation based on fast Fourier transforms for the prediction of the viscoplastic deformation of poly-crystals is used with rate-sensitive crystal plasticity. Two measured polycrystalline structures are used to instantiate the simulations, as well as a fully periodic synthetic polycrystal adapted from a simulation of grain growth. Application of (Euclidean) distance maps shows that hot spots in stress tend to occur close to grain boundaries. It is also found that low stress regions lie close to boundaries. The radial distribution function of the hot spots indicates clustering. Despite the lack of texture in the polycrystals, the hot spots are strongly concentrated in $\langle 1\,1\,0 \rangle$ orientations, which can account for the observed clustering. All three microstructures yield similar results despite significant differences in topology.

(Some figures in this article are in colour only in the electronic version)

1. Introduction

The objective of this paper is to investigate the characteristics of local concentrations of high stress under plastic deformation in ductile single-phase polycrystals. The motivation for the investigation is to learn more about events leading up to the nucleation of damage such as voids in ductile fracture. The hypothesis is that the polycrystalline structure is effectively a composite structure in which each grain affects the deformation of its neighbors and perhaps beyond. It is thus a mesoscale investigation between the scale of individual dislocations and their interactions and the scale of components and stress (or strain) concentration in the engineering sense. We

focus on characterizing hot spots in the stress field, or, more precisely, local fluctuations above the mean stress. One potential application is in stress-based approaches to damage initiation and growth. Other approaches to damage initiation have been explored, generally at the statistical level (as opposed to the detailed examination of full-field solutions as in this work), e.g. the dissipation-based approaches of Przybyla and McDowell [1] and Charkaluk and Constantinescu [2]. Accordingly, we explore a stress-based approach primarily to develop the tools required to understand hot spots in detail. Since full-field solutions are calculated on a regular grid, it seemed important to avoid dealing with the behavior at individual points. Therefore, a threshold is applied to the stress field and the clusters of high stress points in the upper 10% or less of the distribution are used for analysis. Several questions are posed concerning the sizes, spatial arrangements and crystal orientations in the high stress clusters. For examining spatial relationships with microstructural features, (Euclidean) distance maps, e.g. [3], proved useful, for quantifying proximity of hot spots to boundaries, etc. Note that in some circumstances the strain(rate) fields may be more important. In a previous paper on high volume fraction composites [4], for example, it was found that the strain-rate field exhibited the greatest sensitivity to microstructure.

2. Review

Previous work on microstructurally resolved plasticity has addressed a number of issues similar to those examined here. Barbe *et al* [5] found that, whereas the global response is insensitive to mesh refinement, the amplitude of local variations in stress increases slowly with increasing mesh refinement. Diard *et al* [6] performed finite element simulations on polycrystals with properties for hexagonal metals. Although they determined that more than 400 integration points were sufficient to resolve intragranular gradients in stress and strain, they did not arrive at any definite conclusions about the influence of grain boundaries. Kanit *et al* [7] examined the differences arising from using a mesh conformed to the grain structure, i.e. with relatively smooth grain boundaries, versus a voxel-based mesh, i.e. with stair-stepped boundaries. They found only minor differences between the two cases in the local field values. They also noted that great care must be used in determining how large a volume may be regarded as representative, in the sense of demonstrating converged values for properties such as modulus. The dispersion in modulus of thermal conductivity converges significantly more slowly (with numbers of realizations) than the mean values, not surprisingly. In general, the available results of microstructurally resolved simulations show that in single-phase polycrystals, at least, substantial intragranular gradients in stress and strain exist although the grain structure is always apparent in the stress and strain fields. Lewis *et al* [8] used anisotropic elasticity FEM for a 3D microstructure of a commercial stainless steel Al6XN, and investigated correlations of the hot spot (von Mises equivalent stress) distribution, distance to the nearest grain boundary, grain boundary character and imposed loading condition using various visualization and analytical techniques. No clear correlations were found. The spatial distribution of hot spots and its relation to microstructural features vary by imposed loading conditions.

3. Approach and methods

3.1. Technical approach

The approach is to obtain full-field solutions for stress and strain rate using a three-dimensional discrete fast Fourier transform (FFT)-based viscoplastic model that uses an image of the

microstructure of interest as its input. This model has been pioneered by Suquet and collaborators [9–11] and further developed by Lebensohn [12] and collaborators [13–15] for the specific case of viscoplastic polycrystals. The scope of the investigation is limited in this case to uniaxial tensile deformation of randomly oriented polycrystals. A single strain step is applied such that no texture evolution is considered. Two different microstructures are considered in detail with the motivation of investigating sensitivity to grain shape; a third measured microstructure was investigated in less detail. The first was a synthetic microstructure with 426 grains that was obtained from an isotropic Monte Carlo model of grain growth, see [16] for example. This microstructure had equiaxed grains with the size distribution characteristic of such simulations, which means that the spread in size is slightly narrower than typically observed in experiments. The microstructure was discretized on a regular grid, $\{x^d\}$, with size $128 \times 128 \times 128$. Exactly the same grid was used in the grain growth and FFT models and the periodic nature of the prior grain growth simulation was carried over in the microstructure to the FFT model. The second microstructure is derived from serial sections taken through a sample of an IN100 nickel alloy. The processing of the serial sections to produce the 3D image has been described elsewhere [17]. From the original image with dimensions $389 \times 146 \times 184$ (voxels), a subset with dimensions 128^3 was extracted for use in the FFT model. This measured microstructure is, of course, not periodic, which, by contrast to the synthetic microstructure, means that there is a mismatch between grains across the edges of the cell. As we shall see, however, this does not appear to lead to exceptional behavior at the edges of the simulation cell. Orientations for the synthetic microstructure were drawn from a list that represents a uniform (or 'random') orientation distribution or texture. In the measured microstructure, the texture was found to be random, which is reasonable in light of the powder-based fabrication of the material. Finally, a third experimentally derived microstructure, from a serial sectioning experiment on pure nickel, was used to verify the generality of the results. This microstructure was discretized on a grid of size $256 \times 256 \times 32$ in conformance with the available data set. In all the calculations, the critical resolved shear stress was set at one and so the stress values are on an arbitrary scale; an average strain rate of one was imposed on the polycrystal as a whole. $\{1\,1\,1\}\langle 1\,1\,0\rangle$ slip appropriate to fcc metals was used in all calculations.

3.2. FFT method

The FFT-based formulation for viscoplastic polycrystals used in this work for property simulation requires periodic unit cells and provides a solution of the governing differential equations for stress equilibrium and compatibility. The microstructure is discretized on a regular grid $\{x^d\}$, which in turn determines a corresponding grid of the same dimensions in Fourier space $\{\xi^d\}$. An average strain rate $\dot{E}_{ij}$ is imposed on the unit cell and the response to this mechanical boundary condition, in terms of stress and strain-rate fields, is determined. The use of such regular grid means that the resolution, in relation to the microstructural features such as grain size, is limited by the gridpoint spacing.

   The FFT-based formulation has been described in detail in several previous publications [9–15], (in particular, the specialization to viscoplastic polycrystals can be found in [12–15]). Therefore we provide only the essentials of the method and readers are referred to the previous publications for further details.

   The viscoplastic FFT-based algorithm computes a compatible strain-rate field, associated with a kinematically admissible velocity field that minimizes the average work rate and satisfies at every point the constitutive relation with an equilibrated stress field. This constitutive relation

is given by the well-known crystal plasticity rate-sensitive equation:

$$\dot{\varepsilon}(\boldsymbol{x}^{\mathrm{d}}) = \dot{\gamma}_{\mathrm{o}} \sum_{k=1}^{N_{\mathrm{s}}} m^{\mathrm{s}}(\boldsymbol{x}^{\mathrm{d}}) \left(\frac{|m^{\mathrm{s}}(\boldsymbol{x}^{\mathrm{d}}) : \sigma'(\boldsymbol{x}^{\mathrm{d}})|}{\tau_{\mathrm{o}}^{\mathrm{s}}(\boldsymbol{x}^{\mathrm{d}})} \right)^{n} \times \mathrm{sgn}\,(m^{\mathrm{s}}(\boldsymbol{x}^{\mathrm{d}}) : \sigma'(\boldsymbol{x}^{\mathrm{d}})), \quad (1)$$

where the sum runs over all N_{s} slip systems, $\tau_{\mathrm{o}}^{\mathrm{s}}$ and $m^{\mathrm{s}}(\boldsymbol{x}^{\mathrm{d}})$ are the threshold resolved shear stress and the symmetric Schmid tensor associated with slip or twinning system (s), $\dot{\varepsilon}(\boldsymbol{x}^{\mathrm{d}})$ and $\sigma'(\boldsymbol{x}^{\mathrm{d}})$ are the strain-rate and (deviatoric) stress tensors evaluated at the gridpoints, $\dot{\gamma}^{\mathrm{s}}$ is the local shear-rate on slip system (s), $\dot{\gamma}_{\mathrm{o}}$ is a normalization factor and n is the rate-sensitivity exponent.

The FFT-based method relies on the fact that the local mechanical response of a periodic nonlinear heterogeneous medium can be calculated as a convolution integral between Green's function of a linear reference homogeneous medium and a polarization field, which collects both the heterogeneity and the nonlinearity of the actual constitutive response. Since convolution integrals transform to a simple product in Fourier space, the FFT algorithm serves to transform the Green function and the polarization field into Fourier space and, in turn, to get the mechanical fields by back-transforming the product of these two quantities into real space. Given that the polarization that we seek depends precisely on the *a priori* unknown mechanical fields, an iterative scheme is implemented to obtain, upon convergence, a compatible strain-rate field and an equilibrated stress field. Because of the strong mechanical contrast associated with the viscoplastic constitutive relation (equation (1)), the actual iterative procedure used in the simulations presented here employs the augmented Lagrangians algorithm [10, 11]. This more involved methodology (compared with 'basic' FFT scheme of Moulinec and Suquet [9]) updates both an equilibrated stress field and a compatible strain-rate field, along with two auxiliary stress and strain-rate fields (related to each other by the constitutive relation, equation (1)). The simultaneous convergence of (a) the equilibrated and auxiliary stress fields and (b) the compatible and auxiliary strain-rate fields, guarantees that the resulting fields simultaneously fulfill equilibrium and compatibility, respectively (see [11, 15]) for details).

4. Results

As mentioned previously, the result of the calculation is a pair of fields for the stress and strain-rate tensors. Since the calculation is performed for only the deviatoric parts of stress and strain rate, each grid point has a five-component tensor associated with it for each field. In what follows, only the von Mises equivalent stress and strain rate (as scalar quantities) are used for visualization and analysis and are referred to as 'stress' and 'strain rate' without further qualification. Figure 1 shows (*a*) the stress and (*b*) strain rate on the exterior surfaces of the synthetic microstructure. Variations in stress and strain rate appear to be associated with the grain structure with a few grains being either low or high in stress or strain rate. The histograms for (*c*) stress and (*d*) strain rate are approximately normal in shape although there are definite cut-offs at both the lower and upper ends of the distributions that are related approximately to the minimum and maximum Taylor factors [18].

Figure 2 shows (*a*) the stress and (*b*) strain rate on the exterior surfaces of the measured microstructure in the nickel alloy. Variations in stress and strain rate are again associated with the grain structure although in this case the grain structure is less clear in the stress map and hot spots are evident in the strain-rate map. The histogram for (*c*) stress has two peaks and the histogram for (*d*) strain rate, while approximately normal, has a long upper tail, consistent with
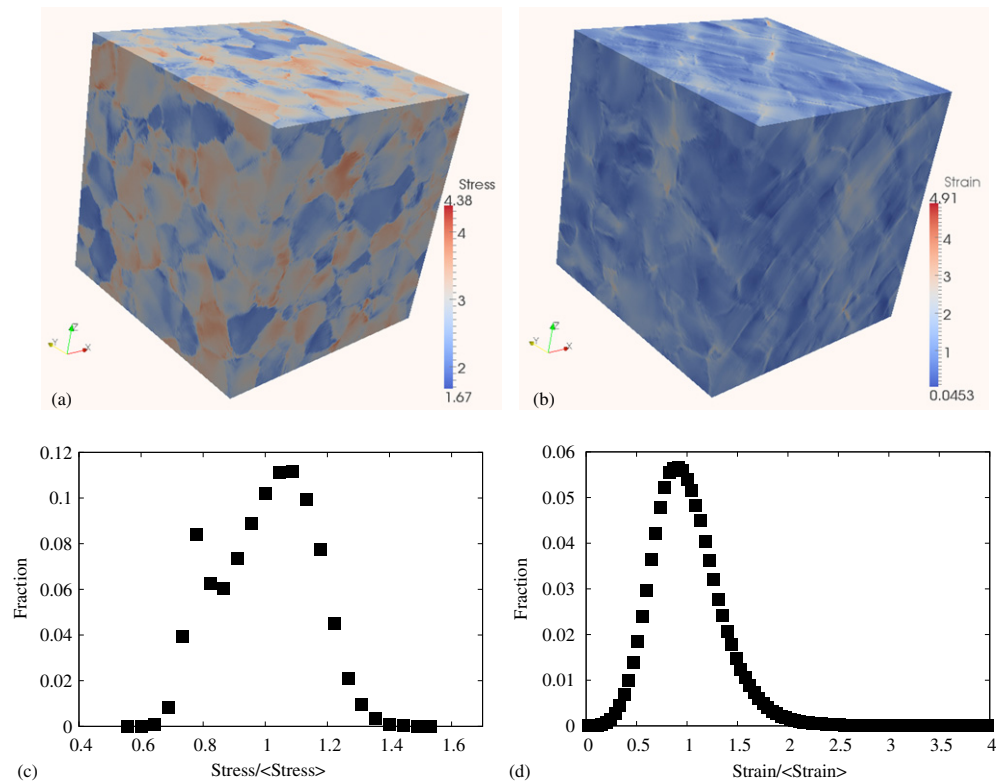
Figure 1. (*a*) Stress field (von Mises equivalent stress) on the surface of the simulation volume for the synthetic polycrystal. The color spectrum indicates stress level from high (red) to low (blue); (*b*) Strain field (von Mises equivalent strain); (*c*) histogram of stresses; (*d*) histogram of strain rate.

the appearance of hot spots. Moulinec and Suquet [19] noted that such extended tails in the histograms of strain rate indicate strain localization. The difference between the single-peak stress histogram for the synthetic microstructure and the less regular histogram with two peaks for the measured microstructure provides the first indication that microstructure can indeed affect the viscoplastic response.

To determine whether or not the application of periodic boundary conditions introduced significant error for the calculations with the (non-periodic) measured microstructure, a plot of average stress on each plane across the simulation volume of the measured polycrystal is shown in figure 3(*a*). More specifically, each of the points labeled 'X' corresponds to the average stress for layers $x_1 = 1, 2, \ldots 128$, and similarly for 'Y' and 'Z'. The lack of an excess or deficit in stress at the edges of the volume (i.e. $x_i = 1$ or 128) suggests that high (or low) stresses are not introduced by the discontinuity in the microstructure, combined with periodic boundary conditions. More specifically, the existence of a plane in each of the three directions across which the grain structure is incompatible might have introduced locally high (or low) stresses but such excess hardness in response is not apparent. The companion figure 3(*b*) shows a cut across the stress field for the measured microstructure and again does not reveal any indications of exceptional behavior near the edges of the simulation cell. This was also discussed for 2D simulations by Lebensohn *et al* [20].
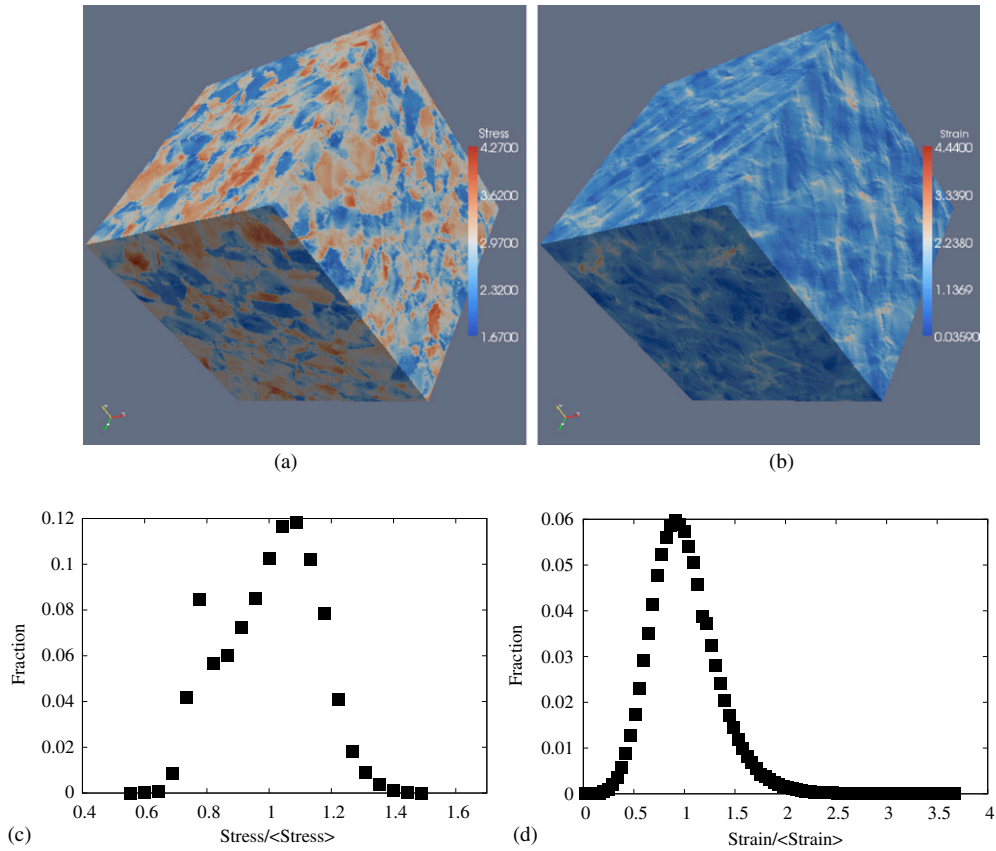
Figure 2. Stress (von Mises equivalent stress) on the surface of the simulation volume for the measured nickel alloy polycrystal. The color spectrum indicates stress level from high (red) to low (blue), via white. (*b*) Strain field (von Mises equivalent strain); (*c*) histogram of stresses ; (*d*) histogram of strain rate. Note the multiple peaks in the stress histogram and the long upper tail in the strain-rate histogram.

4.1. Thresholding

Hot spots were identified by taking super-level sets, X^+, of the von Mises equivalent stress, σ_{vM}, in the sense that only points, x, with values of this field greater than a chosen threshold value, σ_{thresh}, are included in the various analyses:

$$X^+ = X^+(\sigma_{thresh}) = \{x \in \Omega | \sigma_{vM}(x) > \sigma_{thresh}\}. \tag{2}$$

The sizes of the high stress clusters were binned, based on the spherical equivalent radius of each cluster normalized by the average value and excluding clusters with less than two points. The cumulative probability was plotted against the logarithm of the relative size, figure 4. Use of probability paper to make a normal probability plot [21] allows one to test for a (log)normal distribution based on the linearity of the plot. Threshold values in stress were chosen for each microstructure so as to select the upper 5% of voxels ($V_{X^+}/V_\Omega = 0.05$). The size distributions of hot spots are found to be close to log-normal, based on the straightness of the plot, figure 4. Thus the size distributions of the hot spots are quite similar to those observed for the underlying grain structure, given that grain size distributions are commonly found to follow a log-normal distribution [22]. The plots start at substantial fraction because of the presence of many small

(a)   (b)
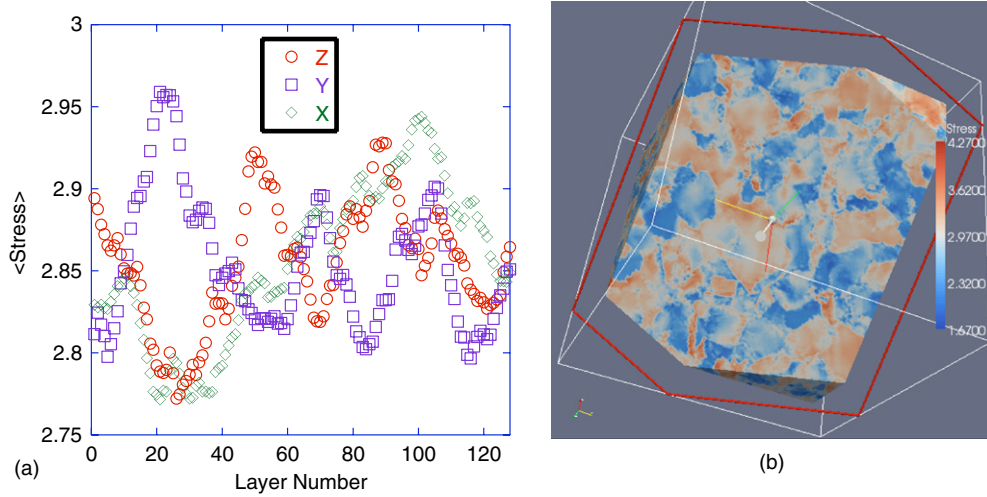
Figure 3. (*a*) Plot of the average stress for each layer of voxels in the measured microstructure, taking sections normal to each of the three grid axes. (*b*) Cut through the simulation volume showing the von Mises stress. Neither figure exhibits exceptional behavior at or near the edge of the simulation domain.
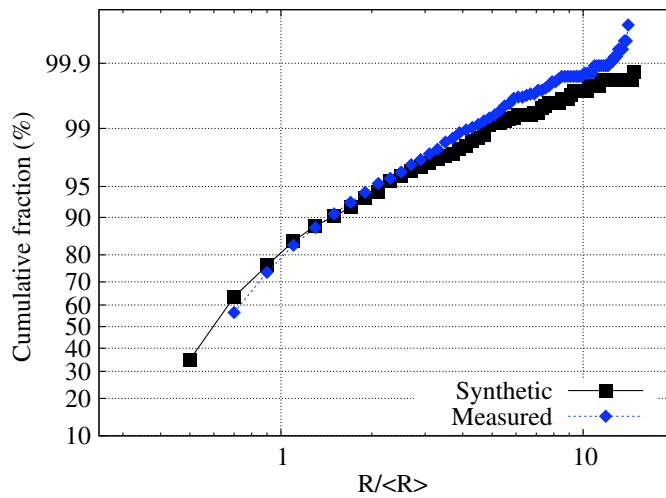

Figure 4. Cumulative probability function for the logarithm of high stress cluster size for a stress threshold that retains 5% of the volume, plotted as probability plot. The straightness of the line indicates that the distribution is close to log-normal, except for the lower tail of the distribution.

clusters in the data sets. This is one of many indications that much larger systems need to be simulated and analyzed in order to obtain statistically meaningful results.

4.2. Stress within hot spots

Figure 5(*a*) shows a plot of the average stress within the thresholded region ($\langle\sigma_{X+}\rangle$) as a function of the log of the volume fraction (V_{X+}/V_{Ω}) for a simulation of uniaxial tension parallel to
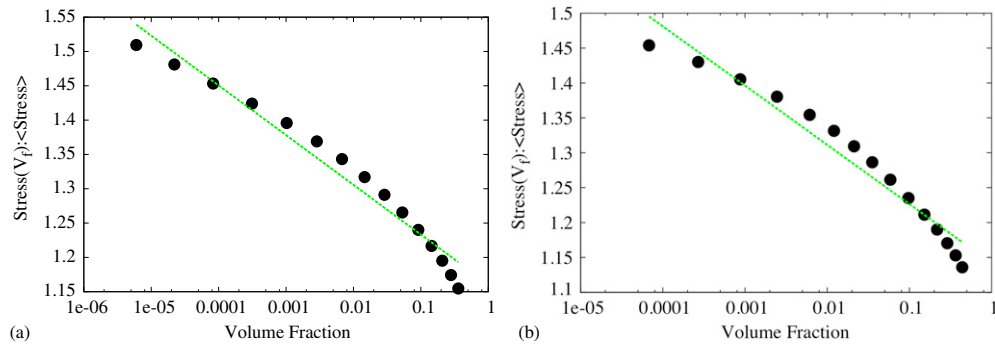
Figure 5. (*a*) Semi-log plot of average stress in high stress clusters, normalized by the average stress for a simulation of uniaxial tension parallel to *Z* in the synthetic polycrystal, versus the volume fraction. The volume fraction of the high stress clusters decreases as the threshold stress increases; (*b*) the same plot for the measured IN100 polycrystal. Note that the stress, as a fraction of the average stress, has to asymptote to the maximum stress in the volume. Nevertheless, there is a finite slope even at small volume fractions, which means that no intercept can be reliably measured.

the *Z*-axis for the synthetic microstructure. The result indicates a roughly semi-logarithmic relationship over a wide range of volume fraction. Nevertheless, the data exhibit curvature over the entire range and, as the volume fraction approaches zero at the left edge, it is not clear that an intercept value can be reliably inferred. Such an asymptote (in stress) might allow a more definite conclusion to be drawn about the relationship between the peak stress and the average stress. Figure 5(*b*) for the measured IN100 microstructure (also uniaxial tension parallel to *Z*) shows a similarly nonlinear relationship. The different (randomly oriented) microstructures yield rather similar responses under the same simple loading conditions. Neither result shows a simple trend.

4.3. Radial distribution function

Figure 6 shows a radial distribution function (RDF) based on the distances between the centers of gravity of the grains in the synthetic polycrystal. The advantage of computing the RDF on a periodic structure obtained from a Monte Carlo grain growth simulation is that no special precautions are required to limit the range of vector lengths considered to lie entirely within the simulation volume. The value of the RDF is zero for small separations and then rises as smallest grain size is reached. The peak is found close to the average grain diameter with a subsequent minimum. Variations in the RDF at larger separations appear to be just noise. The result strongly resembles that of atoms in a liquid, which seems reasonable since grains are only weakly correlated with their neighbors. Large grains, for example, tend to have smaller than average nearest neighbors [23]. As far as the authors are aware, this is the first time that such a result has been presented for grains in a three-dimensional polycrystal.

Figure 7 shows that the RDFs calculated for the thresholded structures at volume fractions of $V_{X+}/V_{\Omega} = 2.5\%$ (points) and 5% (thin line) rise sharply at much smaller separation distances than for the grain centers (heavy line). This indicates that the hot spots tend to be clustered together. Later we note that hot spots are concentrated in certain texture components, which is consistent with this finding of clustering.
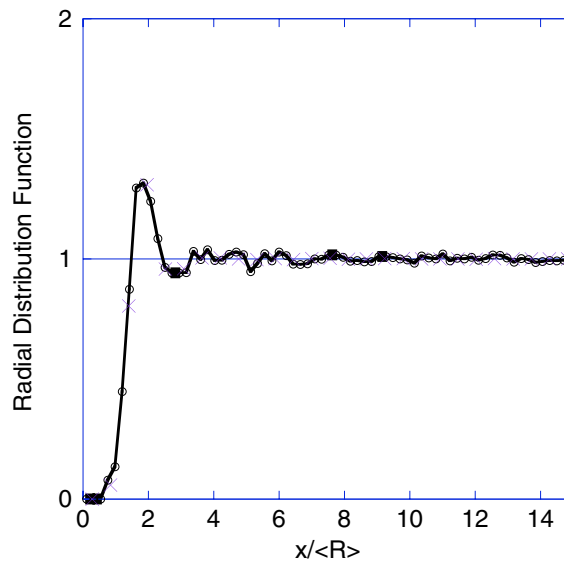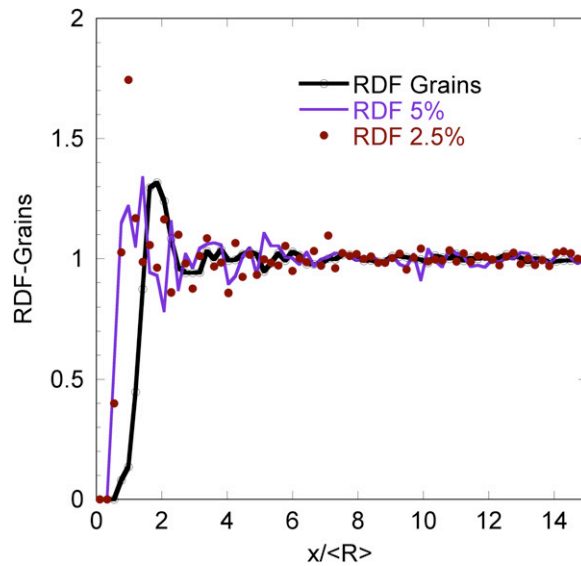
Figure 6. Plot of the RDF for the centers of grains in synthetic polycrystals generated by Monte Carlo simulation of grain growth. Two different grain sizes from different stages in the grain growth process are shown; the circles with line correspond to the synthetic microstructure on which stress–strain computations were performed and the crosses correspond to a structure with about 5000 grains. Note how the RDF is zero up to about 0.5 of the mean grain radius, $\langle R \rangle$, rises rapidly to a peak at about 1.75 $\langle R \rangle$ and then falls to the random value after a shallow minimum at 2.5 $\langle R \rangle$. The two different grain sizes yield very similar results.
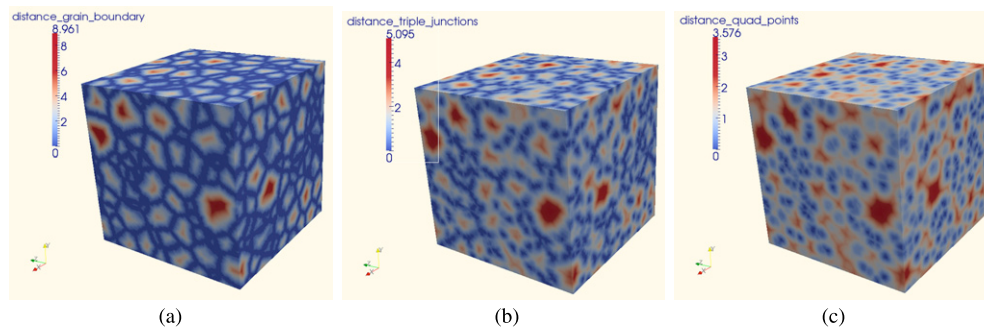
4.4. Distance maps

In order to quantify the spatial relationship between high stress regions and the microstructural features such as grain boundaries, triple lines and quadruple points, a Euclidean distance map (see, e.g. [3]) for each feature was computed for each microstructure. That is to say, for each point, the distance to the closest grain boundary, triple line or quadruple point was computed and stored. To compute such (minimum) distances, it is necessary to classify each voxel based on its neighborhood as being adjacent to a boundary, a triple line, a quadruple point or bulk. Bulk voxels are completely surrounded by voxels of the same orientation; boundary voxels have one or more neighbors with only one different orientation; triple line voxels are adjacent to two different orientations and quadruple points have three unlike neighbors. Since some of the grains are small in terms of the number of voxels across the grain, each non-bulk voxel was treated as belonging to its smallest rank and all others above it. Expressed more simply, a quadruple point also serves as a triple line point and as a boundary point; a triple line point also serves as a boundary point whereas a point with only two unlike neighbors serves as only a boundary point. This ensures that a reasonable ordering of the three distances is always obtained with the grain boundary distance smallest and the quadruple point distance largest. Figure 8 shows examples of distance maps for (a) grain boundaries, (b) triple lines or (c) quadruple points in the synthetic polycrystal.

To analyze the relationship between stress and microstructure, the binning of points by stress is then repeated and the distance values for each feature type are averaged for the points in each bin in the stress histogram. Figure 9(*a*) shows the resulting plot of average distance to (a) boundaries, (b) triple lines or (c) quadruple points for the synthetic polycrystal as a function of stress level for the synthetic microstructure. Each point represents the averaged distance,

Figure 7. The RDFs for the centers of high stress clusters in the synthetic polycrystal are plotted for two different choices of threshold stress that yield volume fractions of 2.5% (solidus) and 5% (thin line). Also plotted is the RDF for the grain centers of the synthetic polycrystal (heavy line with open circles), which rises to a maximum a little below the average grain diameter. The RDF for the clusters rises sharply at a smaller separation, indicating that they are clustered compared with the grain centers.

(a)   (b)   (c)

Figure 8. Distance maps for the synthetic microstructure for (*a*) the distance to the nearest grain boundary (units of voxels), (*b*) the distance to the nearest triple line and (*c*) the distance to the nearest quadruple point. In all three maps, the distances are normalized by the global average value in the structure (to match the normalized distances used in figure 9). The maps emphasize the largest grains in the structure.

normalized by the global average distance, to the nearest feature for points over a certain range of stress, normalized by the global average stress. For grid points with stresses close to the average, the averaged distances are also close to the average values. As the stress increases, the averaged distance decreases, which means, in simple terms, that the highest stress points lie close to microstructural features, as one might expect. It is also the case, however, that points with low stresses also lie close to boundaries, triple lines and quadruple points. This perhaps suggests that not only do grain boundaries give rise to stress concentrations but that shielding can also occur. Figure 9(*b*) shows the equivalent result for the measured polycrystal
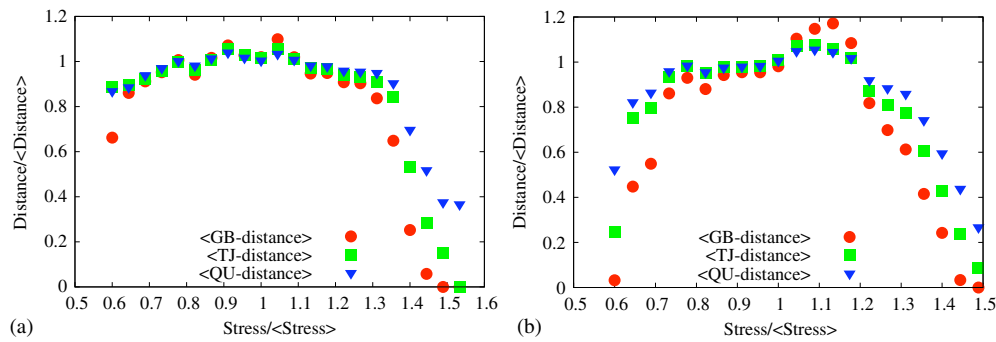
Figure 9. (*a*) Plot of the average distances for the three different microstructural features in each stress class. Data taken from a calculation of uniaxial tension parallel to the *Z*-axis in the synthetic microstructure. (*b*) Plot of the average distances for the three different microstructural features in each stress class. Data taken from a calculation of uniaxial tension parallel to the *Z*-axis in the measured microstructure of IN100.

and the trends are the same. There are slight differences between the two figures, such as the more pronounced peak in all three values above the average stress. Such variations may offer a signature of the differences between different types of microstructure. The variation in the quadruple point distance is less regular but this may be a consequence of the smaller grain size.

4.5. Preferred orientation

Given that the polycrystals modeled both have a random (uniform) texture, one might expect that orientation should play little role in the hot spots, if they are only associated with geometrical features such as grain boundaries. In order to quantify any link, the texture of the retained volume was computed for each threshold stress value. Since the deformation was uniaxial tension, an inverse pole figure on the tension axis is sufficient to quantify the texture. Figure 10 plots the intensity in the $\langle 1\,0\,0 \rangle$ (red), $\langle 1\,1\,0 \rangle$ (green) and $\langle 1\,1\,1 \rangle$ (blue) corners of the unit triangle versus the volume fraction in the high stress clusters in the measured IN100 microstructure for uniaxial tension on the *Z*-axis, with inverse pole figures for selected points to show the overall texture. The basic result is that, as the stress threshold is raised and the volume fraction of the (high stress) clusters decreases, so the texture becomes increasingly concentrated in the $\langle 1\,1\,0 \rangle$ corner of the unit triangle. At lower threshold levels (and larger volume fractions), the $\langle 1\,1\,1 \rangle$ component is dominant, however. It is clear, therefore, that there is a link between the presence of a hot spot and the orientation of the material at that location. Similar results were obtained for uniaxial tension parallel to X and Y in the measured polycrystal and in the synthetic polycrystal.

5. Discussion

5.1. Size distribution

The size distribution of the high stress clusters is interesting for the fact that it is so similar to the approximately log-normal distribution observed for the grains in polycrystalline microstructures. This suggests that it may be interesting to look for correlations between cluster size and the size of the containing grain.
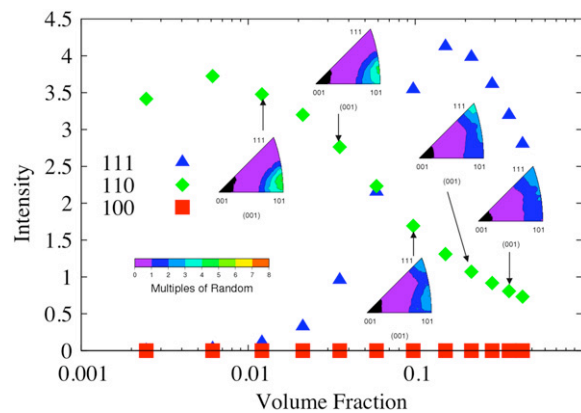
Figure 10. Plot of the intensity in the 1 0 0, 1 1 0 and 1 1 1 corners of the inverse pole figure for the high stress clusters versus volume fraction, calculated as a function of the stress threshold. For selected points, complete inverse pole figures are the inset to show the development of the 1 1 0 fiber texture. Note that the intensity in the 1 1 1 corner rises more rapidly at first with decreasing volume fraction than that in the 1 1 0 corner but then decays away. Data taken from a calculation of uniaxial tension parallel to the Z-axis in the measured microstructure of IN100.

5.2. Hot spot clustering

The result that the RDF for grains is similar to that of amorphous solids is analogous to the Bernal [24] model of atomic structure in liquids. The RDF is widely used in studies of particle packing, e.g. [25], and there is further obvious analogy here. The first peak in the RDF for packed particles, however, typically occurs at one particle (average) diameter, whereas the first peak in the grain center RDF occurs at less than the average grain diameter. Space filling grains can, self-evidently, pack closer together than particles. By contrast, the hot spots are significantly clustered when compared with the grain centers. This result is consistent with the finding that the hot spots tend to be concentrated in the ⟨1 1 0⟩ texture component. This point will be discussed further below.

5.3. Effect of boundaries

Grain boundaries are locations where the crystal orientation changes from one grain to the next, so it is to be expected that the hot spots in stress lie close to boundaries. The Taylor theory of polycrystal deformation is a useful first approximation that says that compatibility for large strains dominates over stress equilibrium; this in turn means that there is, in general, a different multi-axial stress state in each grain in order that multiple slip can occur and the imposed strain be accommodated. At a grain boundary, however, there must be some gradient in stress since neighboring grains have different multiple slip stress states. The result that the trends are similar for both triple lines and quad points to first order is also reasonable because these locations are also where incompatibility in the plastic response is significant. It was somewhat counterintuitive, however, to find that low stress points also lie close to the microstructural features of interest. However, the maps of stress show a number of examples where a high stress grain lies next to a low stress grain. This suggests that the microstructural features can shield certain regions to a certain extent. The possibility of different (neighboring) grains having different load-carrying capacities was discussed by Qidwai *et al* [26].
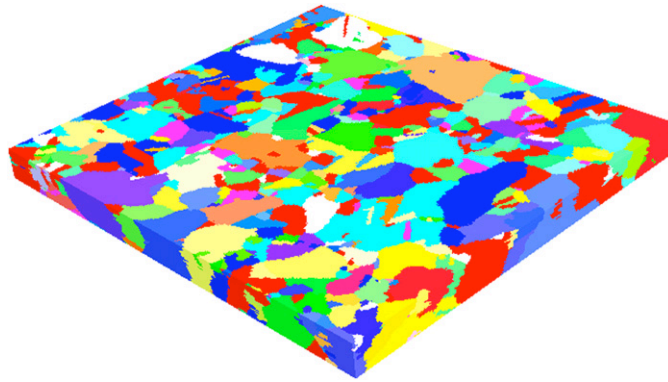
Figure 11. Pure nickel polycrystal sampled by serial sectioning; each grain is colored using a typical inverse pole figure scheme such that red indicates a 1 0 0 plane, green 1 1 0 and blue 1 1 1.

5.4. Crystal plasticity

The strong correlation of high stress points with specific orientations is less surprising than it might at first sight appear. The $\langle 1\,1\,0 \rangle$ corner is a high Taylor factor orientation, meaning that this is where the ratio between the magnitude of the applied stress and the critical resolved shear stress is at a maximum. However, the $\langle 1\,1\,1 \rangle$ corner has the same maximum Taylor factor (for uniaxial tension) as the $\langle 1\,1\,0 \rangle$ corner, with a shallow minimum about halfway in between. At moderate stress threshold levels, both the $\langle 1\,1\,1 \rangle$ and $\langle 1\,1\,0 \rangle$ corners are emphasized in the hot spots, as shown by figure 10. It is only at the highest stress levels that the $\langle 1\,1\,0 \rangle$ corner is strongly selected. As discussed by Hosford [27], the difference between single slip and multiple slip in uniaxial flow reaches its maximum in the 1 1 0 corner of the unit triangle. In the 1 1 1 corner, by contrast, the reciprocal Schmid factor and the Taylor factor as equal, as is also the case in the 1 0 0 corner. This suggests that there is some link between the conflict between single and multiple slip and the occurrence of high stresses in a grain. A previous analysis of intra-grain misorientation development in copper [15] found that the most rapid misorientation development occurred for orientations close to the $\langle 1\,1\,0 \rangle$ corner. This was linked to Dillamore's deformation band development [28, 29] and the ambiguity of orientation change for grains that can rotate towards either the $\langle 1\,1\,1 \rangle$ or the $\langle 1\,0\,0 \rangle$ corner.

5.5. Pure nickel case

A reasonable question is to ask whether the characteristics of the mechanical response of the measured microstructure are specific to that particular sample. Accordingly, we extracted a subset of a similar material, i.e. pure nickel, from a different serial sectioning experiment [30] and performed a similar computation on it. The geometry of the volume characterized, figure 11, was thin and broad, with dimensions $416 \times 374 \times 30$, from which a subset for the simulation grid was extracted with dimensions $256 \times 256 \times 32$. The offset from the edges of the measured volume was 50 voxels in the x and y dimensions and a buffer layer, two layers thick, was added to the z dimension to obtain a cell with power-of-two dimensions. The simulation volume contained 709 grains ranging in size from twenty to 89 232 voxels; grains smaller than twenty voxels were merged with the neighboring grain with the largest contact area with the small grain. The deformation applied was a single strain step of 2% uniaxial tension in the X (sample 1) direction.

13

(a)   (b)
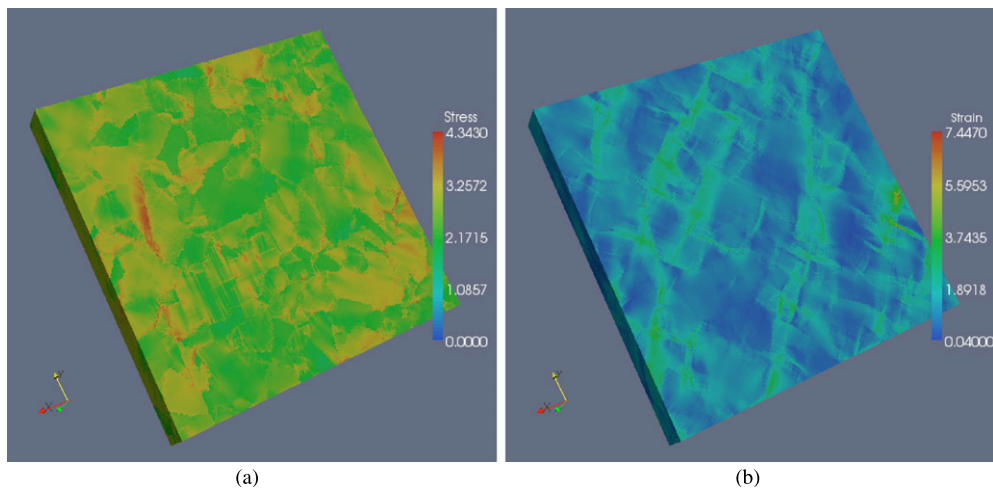
Figure 12. (*a*) Stress (von Mises equivalent stress) on the surface of the simulation volume for the measured pure nickel polycrystal. The color spectrum indicates stress level from high (red) to low (blue), via white. The size of the simulation domain was $256 \times 256 \times 32$. (*b*) Strain rate.
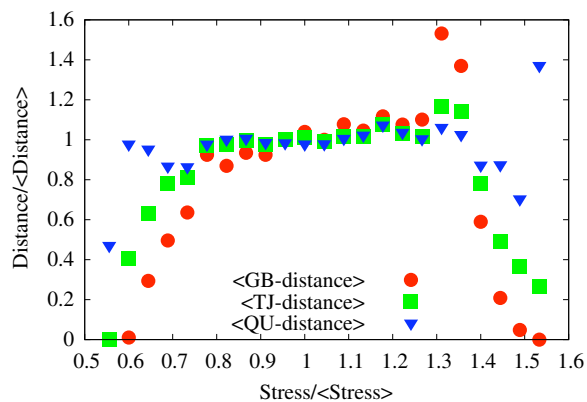
Figure 13. Plot of the average distances for the three different microstructural features in each stress class for the pure nickel microstructure.

Figure 12 shows both (*a*) the stress and (*b*) the strain-rate fields on the surface. Just as with the previous simulations, the grain structure is partially apparent in the stress field. The variation in stress within the high stress (thresholded) regions followed a similar trend to that seen in the nickel alloy case.

Figure 13 shows that the variation in average distance for each of the three microstructural features follows similar trends as seen previously, i.e. that stresses at both the high and low end of the spectrum are located close to grain boundaries, triple lines and quadruple points. There is an upturn in the distance measures for stresses between 1.2 and 1.35 times the mean stress, which is more similar to the IN100 measured microstructure than the synthetic microstructure, which trends downwards from a peak at about $0.9\langle\sigma_{vM}\rangle$. The synthetic microstructure has equiaxed grains, especially by comparison with the two measured microstructures which both have a high density of annealing twins. In both cases the fraction of $\Sigma 3$ boundaries is about 30% by area. In the latter case, however, the measured volume only extends a fraction of the

14

grain size in the *Z*-direction, which means that the grain shapes are not representative of the polycrystal as a whole.

6. Conclusions

Hot spots (in stress), identified by thresholding by stress value, have characteristics that conform to expectations to a certain degree. Use of the distance function quantified statistically the fact that they lie near to microstructural defects such as boundaries, triple lines and quad points. Many of their characteristics are, however, rather similar to the microstructure itself. The hot spot spacings and size distributions are not far different from the grains themselves. The RDF of the grain centers and the cluster centers was examined for the first time. This comparison showed that the RDF of the grain centers is liquid-like and that the hot spots are clustered relative to the grain center spacings. Several additional interesting characteristics were identified. One unexpected result was that low stress points also lie close to defects, suggesting that hot spots in dissipation rate and strain rate should also be investigated. Also, hot spots, developed in an otherwise random texture, have a texture whose strength is inversely related to the threshold level. The texture corresponds to one of the maxima in Taylor factor as a function of orientation in uniaxial tension, namely the 1 1 0 orientation, but the other maximum, 1 1 1, is only associated with hot spots at low values of the threshold stress.

Acknowledgments

References

[1]   Przybyla C P and McDowell D L 2010 Microstructure-sensitive extreme value probabilities for high cycle fatigue of Ni-base superalloy IN100 *Int. J. Plast.* **26** 372–94
[2]   Charkaluk E and Constantinescu A 2009 Dissipative aspects in high cycle fatigue *Mech. Mater.* **41** 483
[3]   Saito T and Toriwaki J I 1994 New algorithms for euclidean distance transformation of an *N*-dimensional digitized picture with applications *Pattern Recognit.* **27** 1551
[4]   Lee S-B, Lebensohn R A and Rollett A D 2010 Modeling the viscoplastic micromechanical response of two-phase materials using fast Fourier transforms, in preparation
[5]   Barbe F, Decker L, Jeulin D and Cailletaud G 2001 Intergranular and intragranular behavior of polycrystalline aggregates: I. F.E. model *Int. J. Plast.* **17** 513
[6]   Diard O, Leclercq S, Rousselier G and Cailletaud G 2005 Evaluation of finite element based analysis of 3D multicrystalline aggregates plasticity—application to crystal plasticity model identification and the study of stress and strain fields near grain boundaries *Int. J. Plast.* **21** 691
[7]   Kanit T, Forest S, Galliet I, Mounoury V and Jeulin D 2003 Determination of the size of the representative volume element for random composites: statistical and numerical approach *Int. J. Solids Struct.* **40** 3647
[8]   Lewis A C, Suh C, Stukowski M, Geltmacher A B, Rajan K and Spanos G 2008 Tracking correlations between mechanical response and microstructure in three-dimensional reconstructions of a commercial stainless steel *Scr. Mater.* **58** 575

 [9] Moulinec H and Suquet P 1998 A numerical method for computing the overall response of nonlinear composites with complex microstructure *Comput. Methods Appl. Mech. Eng.* **157** 69
[10] Michel J C, Moulinec H and Suquet P 2000 A computational method based on augmented Lagrangians and fast Fourier transforms for composites with high contrast *CMES—Comput. Modeling Eng. Sci.* **1** 79–88
[11] Michel J C, Moulinec H and Suquet P 2001 A computational scheme for linear and non-linear composites with arbitrary phase contrast *Int. J. Numer. Methods Eng.* **52** 139
[12] Lebensohn R A 2001 N-site modeling of a 3D viscoplastic polycrystal using fast Fourier transform *Acta Mater.* **49** 2723
[13] Lebensohn R A, Liu Y and Castaneda P P 2004 On the accuracy of the self-consistent approximation for polycrystals: comparison with full-field numerical simulations *Acta Mater.* **52** 5347
[14] Lebensohn R A, Bringa E M and Caro A 2007 A viscoplastic micromechanical model for the yield strength of nanocrystalline materials *Acta Mater.* **55** 261
[15] Lebensohn R A, Brenner R, Castelnau O and Rollett A D 2008 Orientation image-based micromechanical modelling of subgrain texture evolution in polycrystalline copper *Acta Mater.* **56** 3914
[16] Rollett A D and Manohar P 2004 The Monte Carlo method *Continuum Scale Simulation of Engineering Materials* ed D Raabe *et al* (Weinheim, Germany: Wiley-VCH) p 77
[17] Groeber M A, Haley B K, Uchic M D, Dimiduk D M and Ghosh S 2006 3D reconstruction and characterization of polycrystalline microstructures using a FIB-SEM system *Mater. Charact.* **57** 259
[18] Kocks U F, Tomé C and Wenk H-R (ed) 1998 *Texture and Anisotropy* (Cambridge: Cambridge University Press)
[19] Moulinec H and Suquet P 2003 Intraphase strain heterogeneity in nonlinear composites: a computational approach *Eur. J. Mech. A—Solids* **22** 751
[20] Lebensohn R A, Castenau O, Brenner R and Gilormini P 2005 Study of the antiplane deformation of linear 2-D polycrystals with different microstructures *Int. J. Solids Struct.* **42** 5441
[21] *NIST/SEMATECH e-Handbook of Statistical Methods, Normal Probability Plots* (www.itl.nist.gov/div898/handbook/eda/section3/normprpl.htm)
[22] Srolovitz D J, Anderson M P, Sahni P S and Grest G S 1984 Computer simulation of grain growth: II. Grain size distribution, topology and local dynamics *Acta Metall.* **32** 793
[23] Aboav D A 1980 Arrangement of cells in a net *Metallography* **13** 43
[24] Bernal J D 1959 Geometrical approach to the structure of liquids *Nature* **183** 141
[25] Arzt E 1982 The influence of an increasing particle coordination on the densification of spherical powders *Acta Metall.* **30** 1883
[26] Qidwai M A S, Lewis A C and Geltmacher A B 2009 Using image-based computational modeling to study microstructure-yield correlations in metals *Acta Mater.* **57** 4233
[27] Hosford W F 1993 *The Mechanics of Crystals and Textured Polycrystals* (New York: Oxford University Press)
[28] Dillamore I, Morris P, Smith C and Hutchinson W 1972 Transition bands and recrystallization in metals *Proc. R. Soc. Lond.* **329** 405
[29] Dillamore I and Katoh H 1974 The mechanisms of recrystallization in cubic metals with particular reference to their orientation dependence *Metal. Sci.* **8** 73
[30] Li J, Dillon S J and Rohrer G S 2009 Relative grain boundary area and energy distributions in nickel *Acta Mater.* **57** 4304